Biochimica et Biophysica Acta 1788 (2009) 458–469

Contents lists available at ScienceDirect

Biochimica et Biophysica Acta

journal homepage: www.elsevier.com/locate/bbamem

Contribution of electrostatic and structural properties of Kv4.3 S4 arginine residues to the regulation of channel gating

Matthew R. Skerritt, Donald L. Campbell *

University at Buffalo, State University of New York School of Medicine and Biomedical Sciences Department of Physiology and Biophysics Buffalo, New York 14214, USA

ARTICLE INFO

Article history:
Received 3 July 2008
Received in revised form 16 September 2008
Accepted 16 September 2008
Available online 2 October 2008

Keywords:
Kv4.3
S4 domain
Gating
Closed-state inactivation
Recovery

ABSTRACT

Previous work has demonstrated that replacing individual arginine (R) residues in the S4 domain of Kv4.3 with alanine (A) not only altered activation and deactivation processes, but also those of closed-state inactivation (CSI) and recovery. R → A mutants eliminated individual positive charge while substantially reducing side chain volume and hydrophilic character. Their novel effects on gating may thus have been the result of electrostatic and/or structural perturbations. To address this issue, and to gain further insights into the roles that S4 plays in the regulation of Kv4.3 gating transitions, we comparatively analyzed arginine to glutamine (R → Q) mutations at positions 290, 293, and 296. This maneuver maintained positive charge elimination of the R → A mutants, while partially restoring native side chain volume and hydrophilic properties. R → A and R → Q mutant pairs produced similar effects on the forward gating process of activation. In contrast, significant differences between the two substitutions were discovered on deactivation, CSI, and recovery, with the R → Q mutants partially restoring wild type characteristics. Our results argue that modification of individual S4 residue properties may result in altered localized interactions within unique microenvironments encountered during forward and reverse gating transitions. As such, predominant effects appear on the reverse gating transitions of deactivation and recovery. These results are consistent with the proposal that arginine residues in S4 are involved in regulating Kv4.3 CSI and recovery.

1. Introduction

Kv1.4, the mammalian homologue of the Shaker voltage-sensitive potassium channel, and all members of the Kv4 (Shal-type) family generate rapidly activating and inactivating potassium-selective currents in response to membrane depolarization. In association with regulatory β subunits, these channels generate current phenotypes designated I_A in neurons and I_{to} in cardiac myocytes [1–3]. Due to their rapid activation and subsequent inactivation kinetics, both channel types can significantly modulate action potential repolarization and frequency-dependent electrical signaling. I_A/I_{to} has thus been hypothesized to play important functional roles in diverse excitable cell types, including neuronal somatodendritic interactions [1,2,4], long-term potentiation [4,5], pain plasticity [6], and excitation–contraction coupling in smooth and cardiac muscle [1,3,7]. Nonetheless, while Kv1 and Kv4 α subunits give rise to current phenotypes that are similar phenotypically, there are important differences in the molecular, biophysical, and pharmacological characteristics between the two channel families [1–3].

The mechanisms of inactivation and recovery from inactivation in Kv1 channels are now understood in reasonable detail. In contrast, the corresponding mechanisms in Kv4 have yet to be elucidated [1–3]. However, it is known that conventional Shaker-like N- and P/C-type processes are likely not operative [1–3,8,9]. Kv4 channels also display prominent closed-state inactivation (CSI), a process which is minimal in Kv1 [10,11]. With regard to voltage sensitivity and activation, extensive work on Kv1 channels has established that transmembrane segments S1–S4 form the voltage-sensor domain (VSD) [12–16]. Within the VSD, S4 is believed to be responsible for conferring voltage sensitivity. Each S4 domain contains six basic residues, with the first four arginines (R1–R4) providing most of the gating charge [12–18]. Although the exact contribution of each residue to total gating charge movement is unclear, approximately 13 elementary charges (e_0) per channel (3.2 e_0 per α subunit) are moved [12–18].

Little experimental work has been conducted on mechanisms regulating Kv4 channel voltage sensitivity, and how such mechanisms may regulate overall gating transitions. While the general concepts underlying Kv1 voltage sensitivity likely apply to Kv4 [1–3], it is recognized that Kv4 steady-state activation relationships are less voltage-dependent than those of Kv1 [3,9,19–21]. This may be due, in part, to the fact that S4 in Kv4.3 possess less overall positive charge, with Shaker R1 replaced by neutral valine (V) at position 287 (Fig. 1A).

Our laboratory recently demonstrated the involvement of positively charged residues in regulating Kv4.3 gating transitions by mutating arginine to the neutral and more hydrophobic residue alanine, A [21]. Although that study did not provide direct evidence that S4 charged residues contribute to net gating current (for

* Corresponding author. Tel.: +1 1 716 829 2069; fax: +1 1 716 829 2227.
E-mail address: dc25@buffalo.edu (D.L. Campbell).

0005-2736/$ – see front matter © 2008 Elsevier B.V. All rights reserved.
doi:10.1016/j.bbamem.2008.09.012

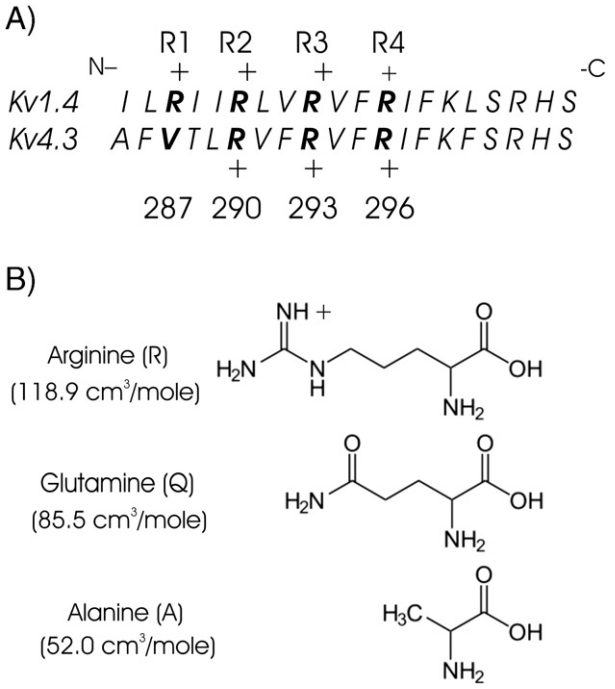

Fig. 1. (A) Sequence comparison of Kv1.4 and Kv4.3 S4 domains. Note that Kv1.4 R1 is absent in Kv4.3 and replaced by neutral valine 287. (B) Structures of arginine (R), glutamine (Q), and alanine (A), and their calculated molar volumes [27]. A is hydrophobic, while R and Q maintain hydrophilic properties.

further discussion see Methods and [13,22–24]), R → A mutation did alter the characteristics of Kv4.3 activation and deactivation in a manner consistent with general predictions of the Kv1 channel model. More surprisingly, the R → A mutants significantly altered the characteristics of Kv4.3 CSI and recovery, an initial novel finding. These observations argue that Kv4.3 closed-state inactivation may possess inherent voltage dependence, in contrast to Shaker N-type inactivation where voltage dependence appears to arise from coupling to activation [10,11,24]. Coupling of CSI to activation may also occur in Kv4.3, albeit by a mechanism unlike that existing in Kv1 channels.

Perturbation of either electrostatic or structural properties in S4 may alter voltage-dependent gating characteristics [23–26]. Previous R → A mutants not only eliminated positive charge of the wild-type residue, but also reduced native side chain volume by 67 cm^3/mol [27] (Fig. 1B) and incorporated less hydrophilic character at the position [28,29]. Combined, these effects may have selectively altered domain interactions within unique microenvironments experienced during various gating transitions [15,16,30–36], and thus be responsible, to a degree, for the noted variation in gating properties [21].

To address these concerns, we have conducted a comparative analysis of corresponding S4 arginine to glutamine mutation (R → Q) at positions 290, 293, and 296 (Fig. 1A). Our motivation was to maintain positive charge elimination of the R → A mutants while partially restoring native side chain volume (R → Q=−33 cm^3/mol [27]) and hydrophilic characteristics (Fig. 1B). R290, R293, and R296 were targeted because they are likely responsible for carrying the majority of Kv4.3 gating charge during channel gating transitions. We found that corresponding R → A and R → Q mutant pairs produced similar effects on activation characteristics, but unique effects on the processes of deactivation, closed-state inactivation, and recovery. Our results suggest that both electrostatic and structural perturbations of individual S4 arginine residues can alter channel gating, and are consistent with the proposal that these residues are involved in the regulation of closed-state inactivation and recovery processes.

2. Methods

2.1. Mutagenesis

Kv4.3 was cloned from ferret heart (long form, GenBank AF454388) as described previously [21,37], and maintained in the pBluescript KS(+) vector. Site directed mutagenesis was performed using the Quick Change II Site-Directed Mutagenesis Kit (Stratagene, La Jolla, CA, USA) and primers designed to arginine residues R290, R293, and R296 (Invitrogen, Carlsbad, CA, USA) in the fourth transmembrane segment, S4. Specificity of mutations was confirmed by sequencing (DNA Sequencing Facility, Roswell Park Cancer Institute, Buffalo, NY, USA).

2.2. In vitro transcription and oocyte preparation

Kv4.3 wild type and mutant clone plasmids were linearized with the restriction endonuclease XhoI (New England Biolabs, Ipswich, MA, USA). cRNA was synthesized by the mMessage mMachine T7 Ultra Kit (Ambion, Austin, TX, USA). cRNA quantity and quality was evaluated by spectroscopy and agarose gel electrophoresis.

All animal protocols were conducted in accordance with the NIH-approved guidelines of the Institutional Animal Care and Use Committee, University at Buffalo, SUNY. Oocytes were obtained from mature female *Xenopus laevis* euthanized by a lethal concentration of 6.0 g/L ethyl-3-aminobenzoate methanesulfonate salt and defolliculated as described previously [21]. Twelve to 24 h after isolation, oocytes were injected with 4–9 ng cRNA (Nanoject II; Drummond Scientific, Broomall, PA, USA). Injected oocytes were incubated for 2–4 days at 18 °C.

2.3. Electrophysiology

Two-microelectrode voltage clamp recordings (GeneClamp 500B, Axon Instruments, Union City, CA, USA) were performed on injected oocytes as described previously [21]. Recordings (22 °C) were conducted in ND96 solution (in mM: 96 NaCl, 2 KCl, 1 $MgCl_2$, 1.8 $CaCl_2$, 5 HEPES, pH = 7.40). All voltage clamp recordings were conducted at the maximal gain of the amplifier (10,000×) and clamp rise time stability settings of 60–120 μs. Currents were acquired (filtered at 1 kHz, digitized at 5 kHz) with a Digidata 1320A 16-bit acquisition system under pCLAMP 9 software control (Axon Instruments).

The 90% voltage-clamp rise time criterion was employed for analysis of activation and deactivation kinetics [20,21,38]. A mean value of $t_{90\%}$ = 1.31 ± 0.09 ms was obtained (n = 68). For the measurement of kinetics of recovery from steady-state closed-state inactivation developed at HP = −100 mV (Fig. 11), a series of P1 prepulses of progressively increasing duration was applied from −110 to −150 mV, 10 mV increments, followed by a one second P2 pulse to +50 mV. Fitting the waveform of the increasing peak P2 currents as a function of time permitted determination of the kinetics of recovery from CSI at each fixed P1 potential.

2.4. Theoretical framework

Comprehensive interpretation of the roles charged residues play in the regulation of voltage-sensitive ion channel gating transitions ultimately requires a combination of gating current and single channel analyses [13,22–24]. Due to the present inability to block Kv4 channels in the open state, gating current studies of native channels have yet to prove feasible. A combined mutation of three residues in the outer pore domain was demonstrated to confer non-native *Charybdotoxin* (CTX) sensitivity to Kv4.2 channels and the ability to measure gating currents [39–41]. However, the mutation itself resulted in a hyperpolarizing shift in the steady-state activation relationship, and comprehensive analysis of closed-state inactivation and recovery characteristics of this mutant has yet to be completed.

Thus, in this study, we employed a standard two state gating model as follows:

Steady-state/Isochronal measurements. For a voltage-sensitive two-state channel transition [either a single closed-state to open-state transition (C → O) or a closed-state to closed-state inactivated transition (C → I_C)] the total free energy change ΔG^0 is equal to the sum of voltage-independent (v_i) and voltage-dependent (electrostatic, *es*) components [23–25]: $\Delta G^0 = \Delta G^0_{vi} + \Delta G^0_{es}$. The voltage-independent term ΔG^0_{vi} corresponds to the change in structural (conformational) free energy in the absence of membrane potential (V=0 mV), while the voltage-dependent term ΔG^0_{es} corresponds to the change in electrostatic free energy. The electrostatic component is given by: $\Delta G^0_{es} = \sum_i^m q_i \delta_i V$), where q_i is the charge of each positively charged S4 residue, δ_i is the fraction of the membrane potential sensed by q_i, and V is the voltage across the membrane. Substituting $\alpha = \sum_{i=1}^m q_i \delta_i$, the total free energy change becomes: $\Delta G^0 = \Delta G^0_{vi} + \alpha V$).

For a single Kv4.3 subunit undergoing an independent C → O transition, the steady-state probability of being in the open state is given by a Boltzmann relationship $P_o = \frac{1}{1 + e^{\frac{\left(\Delta G^0_{vi} + \alpha V\right)}{RT}}}$).

Experimentally, the single subunit steady-state activation relationship "*a*" (constructed from saturating tail current measurements [9,21]) can be best fit as $a = \frac{1}{1 + e^{\frac{-V - V_{1/2}}{k}}}$,where V=membrane potential (mV), $V_{1/2}$=the potential of half-maximal activation (mV), and k=slope factor (mV). At 22 °C, movement of one elementary charge (e_0) across the entire membrane potential (δ_i=1.0) would correspond to k=25.43 mV. The equivalency of the expressions for P_o and "a" therefore gives $\alpha = \frac{RT}{k}$ and $\Delta G^0_{vi} = \frac{V_{1/2}}{k} \cdot RT$.

From this two-state model, three interpretative predictions can be made: i) If perturbation of electrostatic forces (changes in α) predominates, a change in slope factor, k, with minimal alterations in $V_{1/2}$ would be predicted; ii) If perturbation of structural properties predominates, a shift in $V_{1/2}$ with minimal alterations in k would be predicted; and iii) If both electrostatic and structural perturbations are significantly contributing, alterations in both k and $V_{1/2}$ would be expected.

Kinetic measurements. In cases where the overall mean voltage-dependence of the time constants of a kinetic process could be determined, the associated τ–V_m relationships were best-fit as exponential functions of voltage. The associated e-fold change in values allowed estimation of effective q_{min}.

2.5. Potential limitations of analysis

Activation/Deactivation kinetics. We make no quantitative conclusions regarding either activation or deactivation kinetics prior to the mean 90% voltage-clamp rise time ($t_{90\%}$) [21,38], i.e. rapid transitions during the initial membrane capacitive charging period were not resolvable.

Two-state gating model. We acknowledge that a two-state formulation is simplistic, and that its application results in estimates of minimal effective gating charge, q. The limitations and potential ambiguities of such a model are recognized and have been previously discussed [22–25]. That being said, this model provides a well-characterized standard for comparing present results to other relevant Kv4 channel studies.

3. Results

A comparative series of current recordings for wild type (WT) Kv4.3 and Kv4.3 R290Q, R293Q, and R296Q are illustrated in Fig. 2.

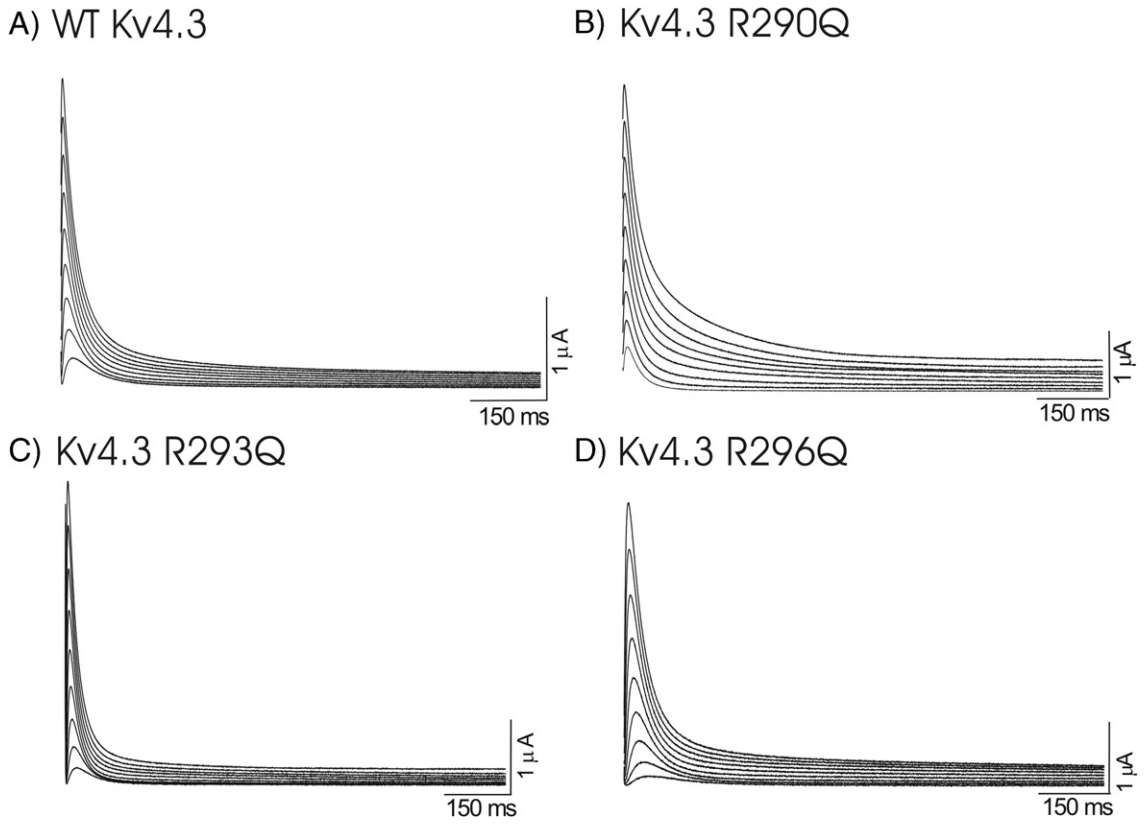

Fig. 2. Representative current recordings for (A) WT Kv4.3, (B) Kv4.3 R290Q, (C) Kv4.3 R293Q, and (D) Kv4.3 R296Q. For all cases, initial HP=−100 mV. For WT, R293Q, and R296Q currents were generated during one second depolarizing voltage clamp step pulses (−30 to+50 mV, 10 mV steps) directly applied from the HP. For R290Q a one second hyperpolarizing prepulse to −150 mV was first applied to remove CSI, followed by one second depolarizing pulses to the depolarized potentials described above.

All constructs gave rise to rapidly activating and subsequently inactivating currents, with amplitudes on the order of 10^{-6} A at +50 mV.

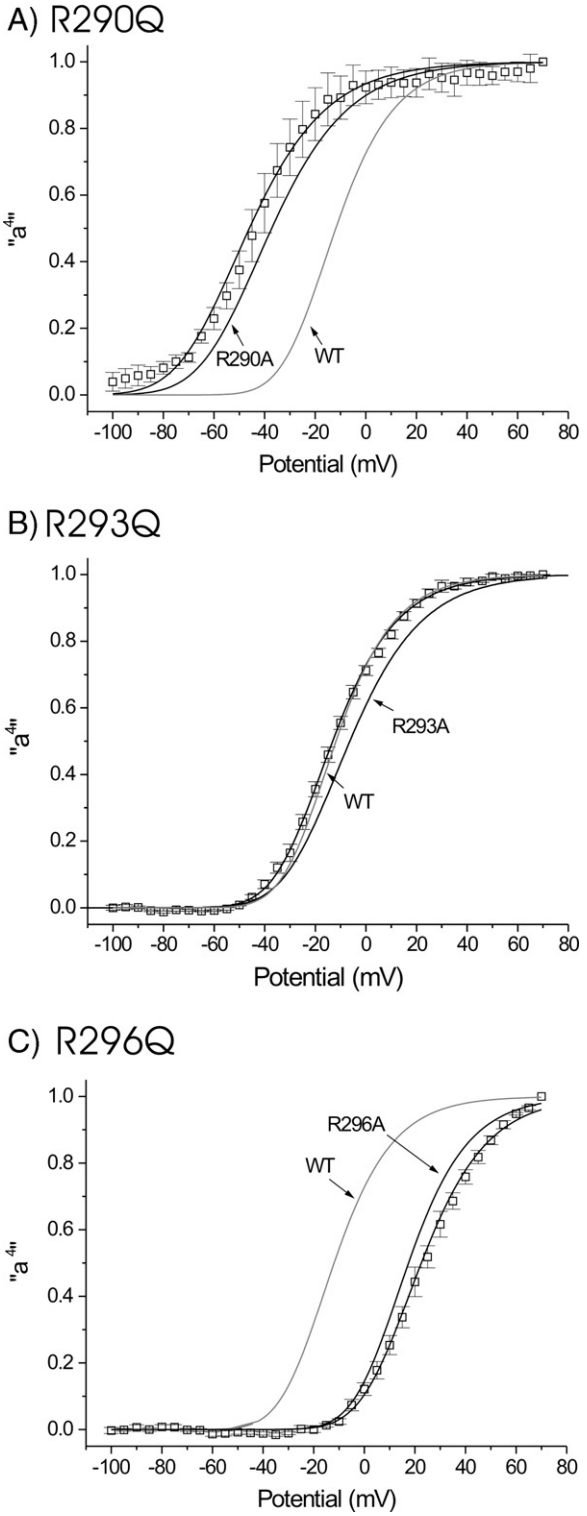

Fig. 3. Mean steady-state activation relationships "a^4" for (A) R290Q (n=9), (B) R293Q (n=9) and (C) R296Q (n=8). Mean data points (±SEM) obtained from normalized peak tail current amplitudes generated from a saturating tail current protocol (HP=−100 mV, P1=10 ms, depolarizing pulses from −95 to +70 mV, 5 mV increments, P2=−50 mV for 1 s, except for R290Q where results from both P2=−50 and −120 mV were pooled [21]). Mean data points fit with a single Boltzmann relationship raised to the fourth power: $\frac{1}{1+e^{\frac{V-V_{1/2}}{k}}}$. Mean fit parameters ($V_{1/2}$, slope factor k) given in Table 1. WT (gray) and corresponding R → A data (black) obtained previously [21].

Table 1
Summary of WT Kv4.3 and S4 R → A and R → Q mutant "a^4" mean fit parameters ($V_{1/2}$: half-activation potential for a single independently activating α subunit; k: single subunit slope factor), minimal q_{act} values (in units of elementary charge e_0 [1.60×10^{-19} C]; values calculated assuming δ_i=1.0), voltage-independent $\Delta\Delta G^0_{Vi}$ values [in units of RT (=0.59 kcal at 22 °C)] and estimated predominant effects of mutants (E: electrostatic perturbations, S: voltage-independent structural perturbations)

	$V_{1/2}$ (mV)	k (mV)	q_{act} (e_0)	$\Delta\Delta G^0_{Vi}$ (RT)	Predominant effect(s)
WT	−36	14.50	1.75	–	–
R290A	−69	19.10	1.33	−1.13	E+S
R290Q	−78	19.20	1.32	−1.58	E+S
R293A	−36	17.80	1.43	+0.46	E
R293Q	−39.5	15.80	1.61	+0.03	E
R296A	−7	14.70	1.73	+2.96	S
R296Q	−4.5	16.25	1.56	+2.76	E+S

3.1. Steady-state activation relationships

Mean steady-state activation relationships "a^4" for R290Q, R293Q, and R296Q are illustrated in Fig. 3A–C. The data points were fit as a single Boltzmann relationship "a" raised to the fourth power

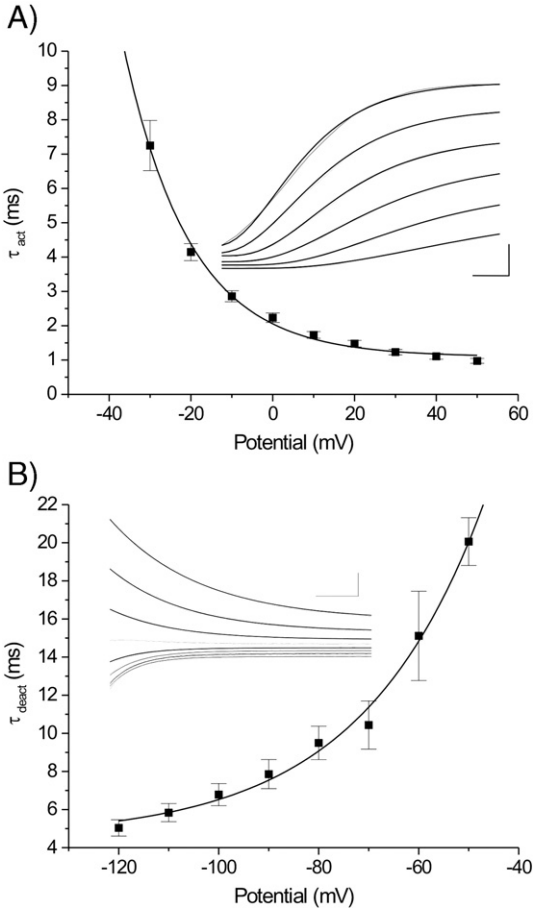

Fig. 4. Voltage-dependence of WT activation and deactivation kinetics. (A) Main panel: Mean τ_{act}–V_m relationship (−30 to +50 mV, n=11). Mean data points fit as a single exponential relationship. Inset: Representative fits of "a^4" activation kinetics for WT currents elicited during depolarizing voltage clamp pulses from 0 to +50 mV, 10 mV increments, HP=−100 mV.τ_{act}=1.8, 1.3, 1.1, 0.9, 0.8, and 0.7 ms, 0 to+50 mV, respectively. $\tau_{90\%}$=1.6 ms for the oocyte illustrated. Calibration bar: 1 μA, 0.5 ms. (B) Main panel: Mean τ_{deact}–V_m relationship (−120 to −50 mV, n=11). Mean data points fit as a single exponential relationship. Inset: Representative single exponential fits (begun at t=2 ms) of WT deactivation kinetics (P1 pulse to +50 mV, 10 ms duration, followed by P2 pulse from −50 to −120 mV, 10 mV increments, 500 ms duration). τ_{deact}=10.5, 8.8, 7.1, 4.0, 3.7, 3.4, and 3.1 ms, −50 to −120 mV, respectively, −80 mV not fit. Calibration bar: 200 nA, 5 ms. Curve fits: (A) Main panel:$\tau_{act}=38.36\,e^{\frac{80-mV}{16.27}}+1.09$ ms; (B) Main panel: $\tau_{deact}=0.74\,e^{\frac{mV}{24.49}}+4.51$ ms.

(independent gating assumed) [9,19,21,42]. For comparison, mean "a^4" fits previously determined for WT and corresponding R → A mutants are also illustrated [21]. Although there were specific quantitative differences (Table 1), R → A/Q mutant pairs displayed similar trends on $V_{1/2}$ values. R290A and R290Q significantly hyperpolarized "a^4", R293A and R293Q produced minimal shifts, and R296A and R296Q significantly depolarized "a^4". Mutant pairs at position 290 thus stabilized the open state, those at 293 resulted in minimal effects, and mutation at R296 stabilized (non-inactivated) closed states.

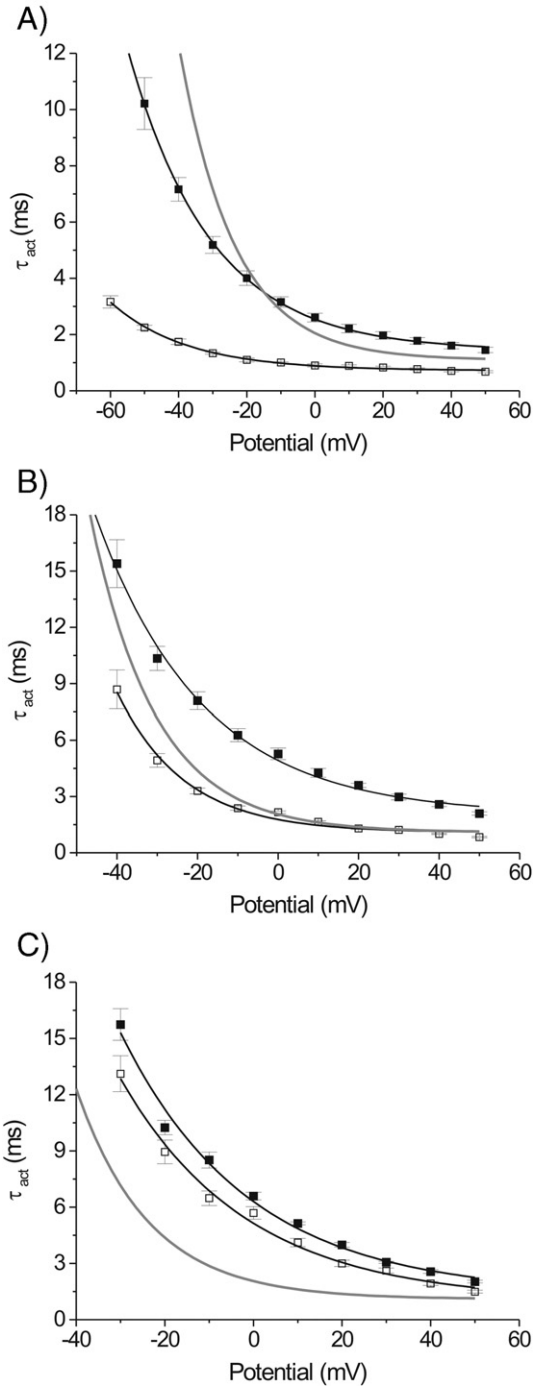

Fig. 5. Voltage-dependence of activation kinetics of corresponding R → A (solid), R → Q (hollow), and WT (gray). (A) R290A (n=13) and R290Q (n=4), (B) R293A (n=9) and R293Q (n=7), and (C) R296A (n=7) and R296Q (n=7). Mean data points fit as single exponential functions of voltage. Kinetic estimates of mean q_{act} summarized in Table 2. Curve fits: (A) R290A: $19.86\,e^{\frac{70-mV}{24.38}}$ + 1.42 ms; R290Q: $2.43\,e^{\frac{60-mV}{22.52}}$ + 0.72 ms (B) R293A: $40.30e^{\frac{70-mV}{26.56}}$ + 2.03 ms; R293Q: $6.39\,e^{\frac{40-mV}{21.70}}$ + 0.90 ms (C) R296A: $13.92\,e^{\frac{30-mV}{28.80}}$ + 1.39 ms; R296Q: $11.87\,e^{\frac{30-mV}{28.55}}$ + 0.99 ms.

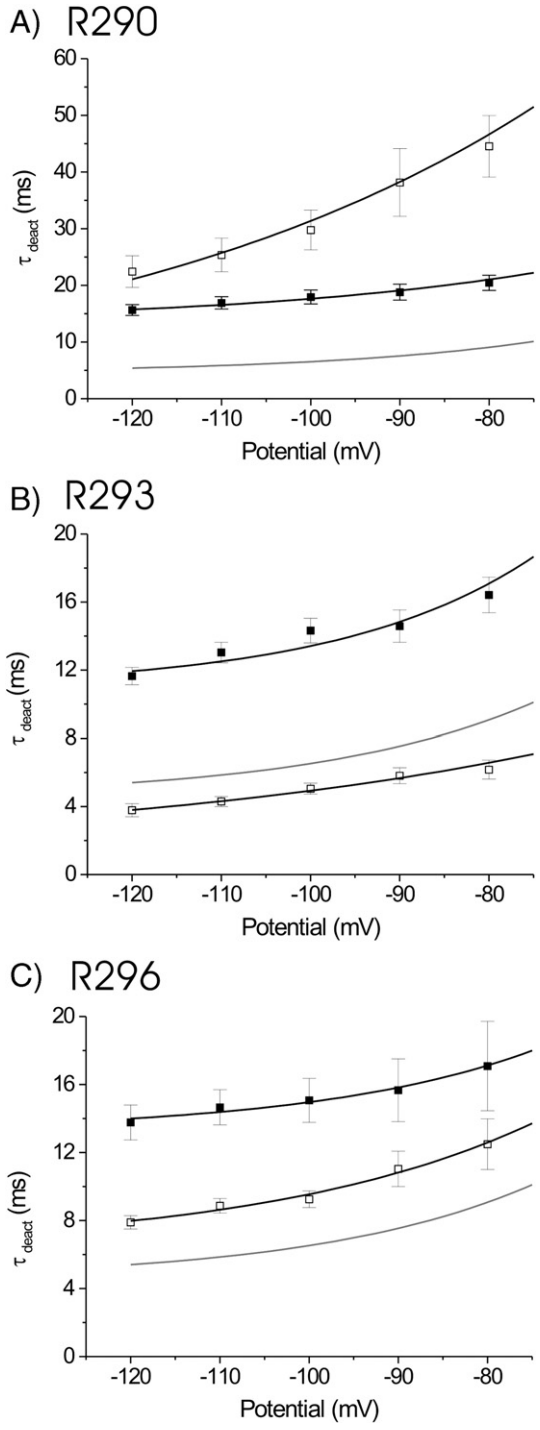

Fig. 6. Voltage-dependence of deactivation kinetics of corresponding R → A (solid), R → Q (hollow), and WT (gray). (A) R290A (n=17) and R290Q (n=10), (B) R293A (n=10) and R293Q (n=10), and (C) R296A (n=8) and R296Q (n=7). Mean data points fit as single exponential functions of voltage. Kinetic estimates of mean q_{deact} are summarized in Table 2. Curve fits: (A) R290A: $1.54\,e^{\frac{mV}{34.41}}$ + 13.34 ms; R290Q: $8.13e^{\frac{mV}{50.80}}$ + 0.28 ms (B) R293A: $0.93e^{\frac{mV}{21.89}}$ + 10.95 ms; R293Q: $1.39e^{\frac{mV}{53.42}}$ + 1.31 ms (C) R296A: $0.62\,e^{\frac{mV}{24.74}}$ + 13.22 ms; R296Q: $0.64\,e^{\frac{mV}{30.30}}$ + 6.29 ms.

A mean value of effective activation gating charge of q_{act}=1.75 e_0 per subunit was obtained for the WT channel. Relative to this value, R → A/Q mutant pairs yielded results that appeared to be dependent upon their position within S4. N-terminal-most R290A and R290Q each reduced q_{act} by 24%. R293A and R293Q reduced q_{act}, though to lesser extents (R293A: 18%, R293Q: 8%). Effects at C-terminal-most R296 were more variable, with R296A resulting in a minimal reduction in q_{act} (1%) and R296Q reducing q_{act} by 11%.

3.2. Activation and deactivation kinetics

Wang et al. [19] have previously demonstrated that Kv4.3 inactivation kinetics were sufficiently slow so as not to obscure activation kinetics. We therefore analyzed the kinetics of activation using a direct-fit Hodgkin–Huxley-like independent "a^4" relationship [21,42]. Representative WT fits are illustrated in Fig. 4A inset. The overall mean WT τ_{act}–V_m relationship (Fig. 4A, main panel) was fit as a single exponential function, from which a kinetic estimate of q_{act} = 1.56 e_0 was obtained. WT deactivation kinetics (−50 to −120 mV) could be well described as a single exponential process [19–21] (Fig. 4B, inset). The overall mean τ_{deact} –V_m relationship was fit as a single exponential function, with q_{deact}=1.04 e_0 (Fig. 4B, main Panel).

The mean comparative τ_{act} –V_m and τ_{deact} –V_m and relationships for each R → A/Q mutant pair are illustrated in Figs. 5 and 6, respectively. Each relationship was fit as a single exponential function, from which the kinetic estimates of q_{act} and q_{deact} were obtained (Table 2).

The R → A/Q mutant pairs differentially altered activation kinetics (Fig. 5). Effects were again dependent upon relative position within S4. Although the largest differences between τ_{act} values were observed at position 290 (Fig. 5A), both R290A and R290Q reduced the voltage-dependence of the τ_{act}–V_m relationship and similarly reduced q_{act} (R290A: 33%, R290Q: 28%). Effects at position 293 were more variable (Fig. 5B). R293A slowed activation kinetics and reduced q_{act} by 38.5%, while R293Q minimally affected activation kinetics and reduced q_{act} by 25% (Fig. 5B). Both R296A and R296Q slowed activation kinetics to similar extents (Fig. 5C) and correspondingly reduced q_{act} by 44%.

The R → A/Q mutant pairs differentially altered deactivation kinetics (Fig. 6). R290A and R290Q each slowed deactivation kinetics and reduced q_{deact} (R290A: 29%, R290Q: 52%, Fig. 6A). Effects at position 293 were heterogeneous. R293A slowed deactivation kinetics and increased q_{deact} by 10%, while R293Q accelerated deactivation kinetics and reduced q_{deact} by 54% (Fig. 6B). Effects at position 296 were also variable (Fig. 6C). R296A slowed deactivation kinetics and minimally reduced q_{deact}, whereas R296Q slowed deactivation kinetics to a lesser extent and reduced q_{deact} by 19% (Fig. 6C).

In summary, despite quantitative differences (Tables 1 and 2), the results generally indicated that, depending upon the relative position within S4, the corresponding R → A/Q mutants exerted overall similar effects on the forward gating process of activation, but more variable effects on the reverse process of deactivation.

3.3. Isochronal inactivation relationships "i"

Mean isochronal (one second) inactivation relationships "*i*" (fit as single Boltzmann relationships) for corresponding R → A/Q mutant pairs are illustrated in Fig. 7.

In contrast to the similar effects that the corresponding mutant pairs produced on "a^4" (Fig. 3), their effects on "*i*" were more variable. R290A/Q and R293A/Q pairs both hyperpolarized "*i*", thereby stabilizing inactivated closed-states (Fig. 7A, B). However, while R296A also hyperpolarized "*i*", R296Q resulted in minimal shift (Fig. 7C). For WT, a mean value q_{csi}=4.10e_0 was obtained. As summarized in Table 3, while there was no apparent dependence upon the relative position in S4, all mutants reduced q_{csi}, from 17% (R293Q) to 58% (R296A). Therefore, with the notable exception of R296Q whose predominant perturbation appeared to be on electrostatic properties of the native residue, all mutants significantly stabilized inactivated closed-states. This indicates

Table 2
Kinetic estimates of q_{act} and q_{deact}

	q_{act} (e_0)	q_{deact} (e_0)
WT	1.56	1.04
R290A	1.04	0.74
R290Q	1.13	0.50
R293A	0.96	1.16
R293Q	1.17	0.48
R296A	0.88	1.03
R296Q	0.89	0.84

Units in e_0 as per Table 1.

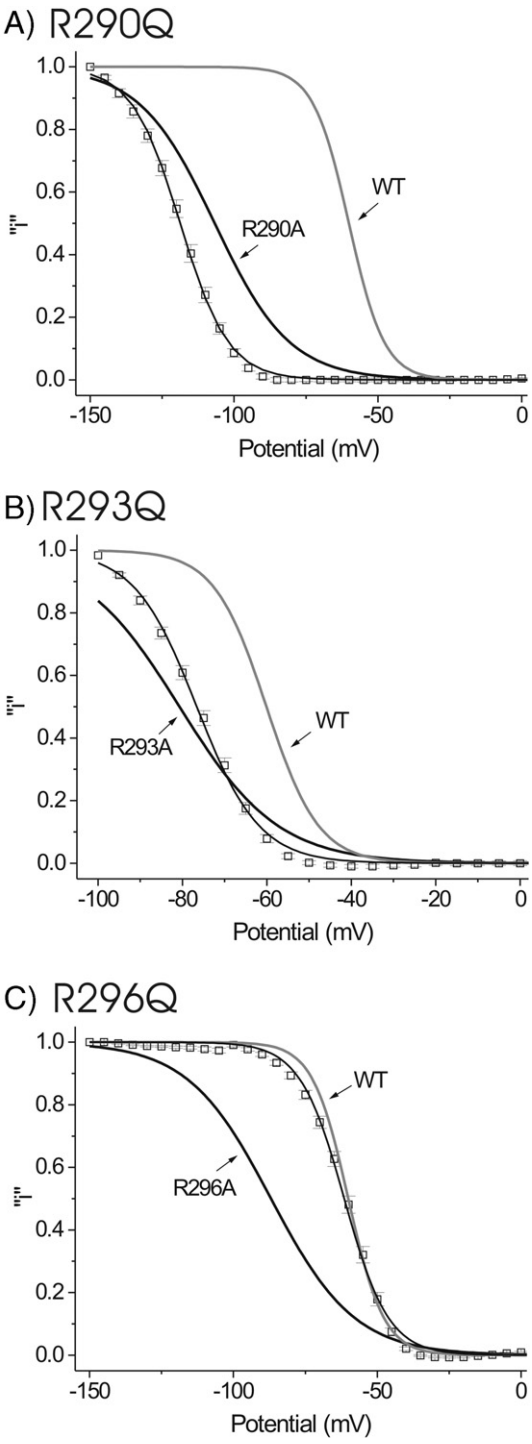

Fig. 7. One second isochronal inactivation relationships. (A) R290Q, (B) R293Q, and (C) R296Q. Mean "*i*" data points fit to a single Boltzmann relationship with parameters summarized in Table 3. Also illustrated in each panel are the corresponding R → A (black) and WT (gray) mean "*i*" relationships obtained previously [21]. R → Q data points fit to single Boltzmann relationships with the following parameters: R290Q:$V_{1/2}$=−118.7 mV, k=8.35 mV (n=9); R293Q: $V_{1/2}$=−80.7 mV, k=11.7 mV (n=10); and R296Q: $V_{1/2}$=−61.5 mV, k=7.71 mV (n=14).

Table 3
Summary of one second isochronal "*i*" fit parameters ($V_{1/2}$: half-inactivation potential; *k*: slope factor), minimal q_{csi} values (calculated assuming $\delta_i = 1.0$, units of e_0), voltage-independent $\Delta\Delta G^0_{vi,csi}$ values (units of RT) and estimated predominant effects of mutants (terminology as per Table 1)

	$V_{1/2}$(mV)	*k* (mV)	q_{csi}	$\Delta\Delta G^0_{vicsi}$	Predominant effect(s)
WT	−60.10	6.20	4.10	–	E+S
R290A	−106.70	13.10	1.94	+1.54	E+S
R290Q	−118.70	8.40	3.03	−4.44	E+S
R293A	−80.70	11.70	2.17	+2.79	E+S
R293Q	−76.60	7.40	3.44	−0.66	E+S
R296A	−86.90	14.50	1.75	+3.70	E+S
R296Q	−61.50	7.70	3.30	+1.70	E

that their effects were likely due to perturbation of both electrostatic and structural characteristics of the native channel.

In summary, in contrast to their effects on "a^4" (Fig. 3), the individual mutant pairs produced distinct alterations in "*i*". CSI could thus be modulated significantly by reduction in S4 net positive charge and alteration of native residue properties. These results argue that mechanisms governing CSI in Kv4.3 either possess inherent voltage dependence or are coupled to inactivation by a mechanism unique from Kv1 channels.

3.4. Macroscopic inactivation and recovery kinetics

Previous analysis revealed that R → A mutation resulted in an overall slowing of macroscopic inactivation kinetics at +50 mV (fit as a double exponential process). While there was alteration in both the fast (τ_{fast}) and slow (τ_{slow}) time constants, the slowing was primarily due to reduction in the relative initial amplitude of the fast component A_{fast} [21]. In the present study, the kinetics of macroscopic inactivation [one second pulse to +50 mV applied from HP=−100 mV (R293Q, R296Q) or following a one second prepulse to −150 mV to remove closed-state inactivation (R290Q)] could again be well described as a double exponential process at potentials depolarized to 0 mV (Fig. 8A, B). Compared to the R → A mutants, corresponding R → Q constructs produced moderate effects on macroscopic inactivation kinetics. R290Q slowed the process, largely due to reduction in A_{fast}. Both R293Q and R296Q produced a net acceleration of inactivation, primarily the result of an increase in A_{fast} (Fig. 8C).

The τ_{inact} – V_m relationships for WT macroscopic inactivation are illustrated in Fig. 9A. Both relationships were fit as single exponential functions, yielding WT values of $q_{inact,fast}$=2.36 e_0 and $q_{inact,slow}$=0.64 e_0. Corresponding relationships for the R → A/Q mutant pairs are illustrated in Fig. 9B–D. While the values of τ_{fast} could be well described beginning at −40 mV for all mutant pairs, τ_{slow} values could only be determined reliably at more depolarized potentials, with the voltage range dependent upon the particular mutant analyzed.

With the exception of R290Q (whose $\tau_{inact,fast}$ –V_m relationship was nearly voltage independent, Fig. 9B), all mutants reduced the voltage-dependence of the relationship and correspondingly reduced $q_{inact,fast}$ values (Table 4). Best fit estimates of minimal q_{slow} are also summarized in Table 4.

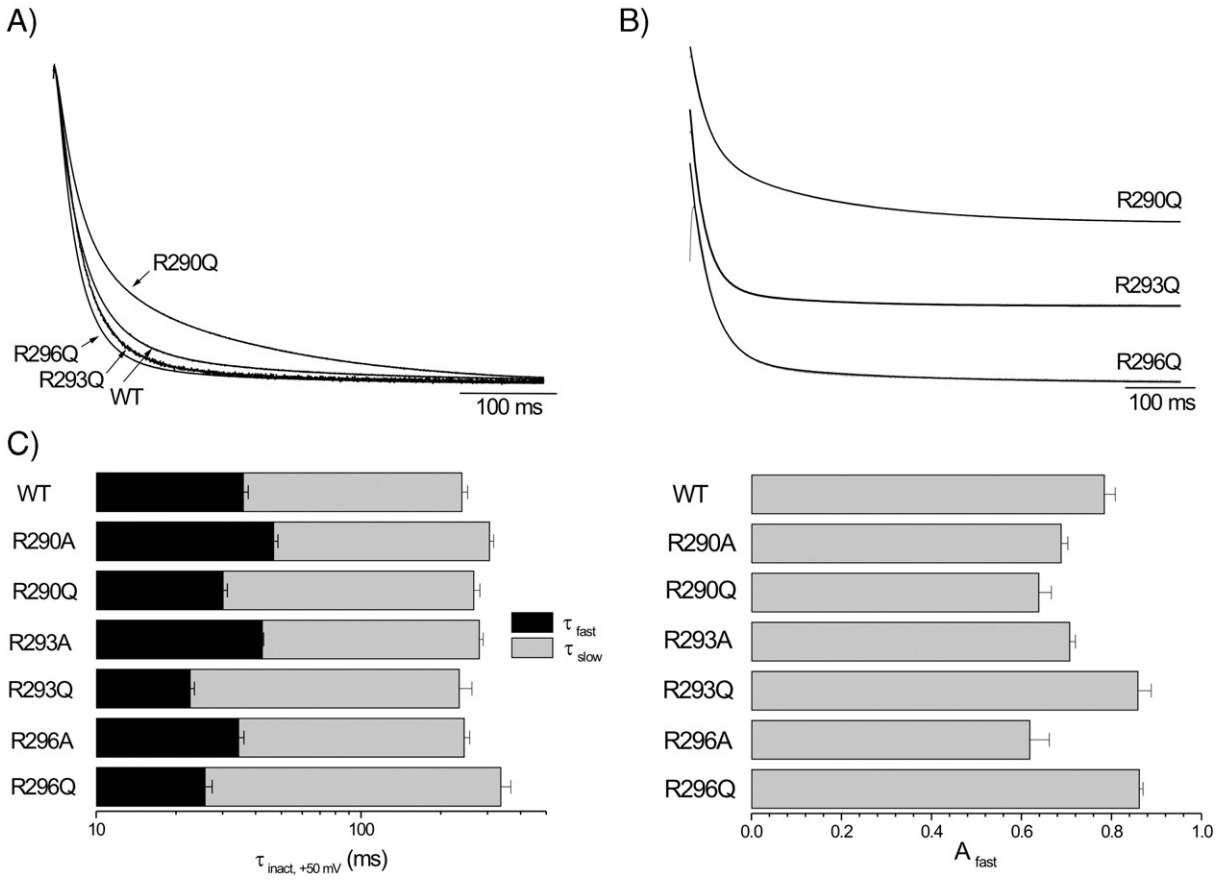

Fig. 8. Macroscopic inactivation kinetics at +50 mV. (A) Overlay of peak currents at +50 mV, current amplitudes normalized. WT, R293Q, and R296Q currents generated during one second depolarizing pulses to +50 mV applied directly from HP=−100 mV. R290Q current generated after a one second hyperpolarizing prepulse to −150 mV to remove CSI. (B) Representative double exponential fits for R290Q, R293Q, and R296Q, current amplitudes normalized. (C) Comparison of the mean time constants (τ_{fast}, τ_{slow}) and initial amplitude of the fast component of inactivation (A_{fast}) at +50 mV. WT and R → A data obtained previously [21]. R → Q mutant data based upon: R290Q (n=5), R293Q (n=7), and R296Q (n=9). Curve fits: (B) R290Q: τ_{fast}=24.0 ms, τ_{slow}=177 ms, A_{fast}=0.62; R293Q: τ_{fast}=20.10 ms, τ_{slow}=134 ms, A_{fast}=0.90; R296Q: τ_{fast}=28.2 ms, τ_{slow}=232 ms, A_{fast}=0.88.

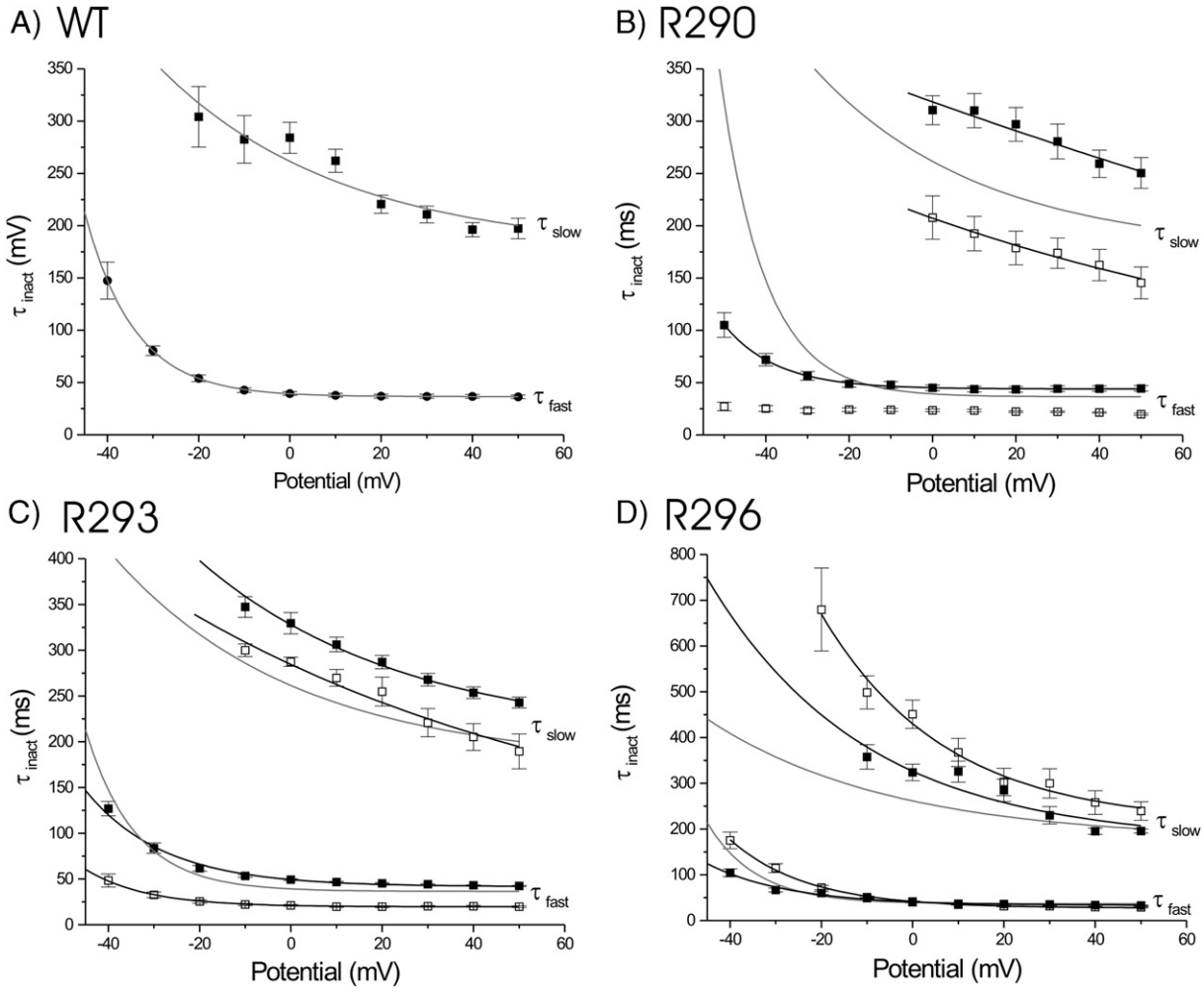

Fig. 9. Mean τ_{inact} -V_m relationships for (A) WT ($n=11$), (B) R290A (solid, $n=11$) and R290Q (hollow, $n=16$), (C) R293A (solid, $n=9$) and R293Q (hollow, $n=11$) and (D) R296A (solid, $n=6$) and R296Q (hollow, $n=9$). For reference, gray curves in (B), (C), and (D) correspond to mean WT data from Panel A. Further details provided in Table 4. Curve fits: (A) WT: $\tau_{fast} = 711.24\,e^{\left(\frac{60-mV}{10.77}\right)} + 36.5$ ms, $\tau_{slow} = 385.1\,e^{\left(\frac{60-mV}{39.95}\right)} + 175.85$ ms (B) R290A: $\tau_{fast} = 61.23\,e^{\left(\frac{50-mV}{12.65}\right)} + 43.9$ ms, $\tau_{slow} = 606.9\,e^{\left(\frac{50-mV}{373.2}\right)} + 212.25$ ms; R293Q: τ_{fast} not fit, $\tau_{slow} = 260.4\,e^{\left(\frac{50-mV}{123.8}\right)} + 33.4$ ms, (C) R293A: $\tau_{fast} = 140.5\,e^{\left(\frac{50-mV}{17.15}\right)} + 41.71$ ms, $\tau_{slow} = 193.3\,e^{\left(\frac{20-mV}{44.5}\right)} + 204.6$ ms; R293Q: $\tau_{fast} = 59.7\,e^{\left(\frac{50-mV}{13.26}\right)} + 19.64$ ms, $\tau_{slow} = 372.14\,e^{\left(\frac{50-mV}{95.44}\right)} + 64.11$ ms (D) R296A: $\tau_{fast} = 208.5e^{\left(\frac{60-mV}{18.04}\right)} + 33.4$ ms, $\tau_{slow} = 892.9e^{\left(\frac{60-mV}{39.95}\right)} + 171.27$ ms; R296Q: $\tau_{fast} = 149.2\,e^{\left(\frac{400-mV}{16.98}\right)} + 27.4$ ms, $\tau_{slow} = 458.2\,e^{\left(\frac{20-mV}{27.03}\right)} + 211.5$ ms.

We previously demonstrated that both R293A and R296A significantly slowed recovery from macroscopic inactivation (HP=−100 mV) developed during a one second depolarizing pulse to +50 mV [21]. Comparative macroscopic measurements were conducted for R293Q and R296Q (Fig. 10). Similar to the R → A mutants, both R293Q and R296Q slowed recovery (fit as a single exponential) (Fig. 10A). However, the mean time constants (R293Q: $\tau_{rec}=593\pm127ms$, $n=6$; R296Q: $\tau_{rec}=1005\pm52ms$, $n=8$) were significantly faster than the corresponding alanine substitutions (Fig. 10B). Thus, partial restoration of native side chain properties at these positions partially restored WT recovery characteristics.

Table 4
Kinetic estimates of $q_{inact,fast}$ and $q_{inact,slow}$

	$q_{inact,fast}$ (e_0)	$q_{inact,slow}$ (e_0)
WT	2.36	0.64
R290A	2.01	0.07
R290Q	ND	0.21
R293A	1.48	0.57
R293Q	1.92	0.27
R296A	1.41	0.74
R296Q	1.50	0.94

ND: not determined. Units in e_0 as per Table 1.

3.5. Closed-state inactivation (CSI) and recovery

Due to the large degree of CSI produced at −100 mV by R290Q (Fig. 7A), it was not possible to obtain comparative macroscopic recovery measurements at this potential. Additionally, it was not possible to maintain sustained hyperpolarized potentials due to rapid oocyte deterioration. However, based upon the R290A/Q "*i*" relationships, it was predicted that both mutants would have displayed CSI recovery kinetics at potentials transiently hyperpolarized to −100 mV. This prediction was tested by applying the following voltage-clamp protocol: from HP=−100 mV, a series of P1 pulses of increasing duration were applied to a fixed hyperpolarized potential ranging from −110 to −150 mV, 10 mV increments, followed by a P2 pulse to +50 mV. Analysis of the peak P2 current amplitudes as a function of P1 duration allowed determination of the voltage-dependence of recovery from steady-state CSI developed at HP=−100 mV.

Consistent with these predictions, at each fixed P1 potential R290A and R290Q displayed significant recovery from CSI developed at HP=−100 mV. The time courses of recovery from CSI were well described as single exponential processes (Fig. 11A). At all P1 potentials the mean $\tau_{rec,\ csi}$ value for R290Q was faster than that of R290A. Single exponential fits to the $\tau_{rec,\ csi}$–V_m relationships

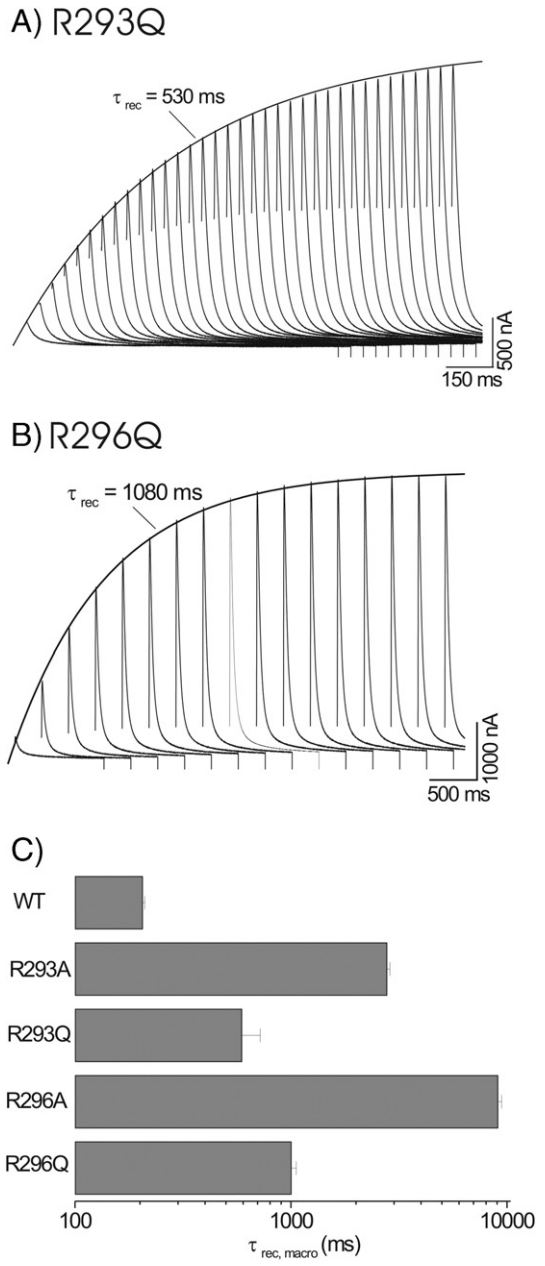

Fig. 10. R293A/Q and R296A/Q macroscopic recovery kinetics at HP=−100 mV. Representative macroscopic recovery waveforms for R293Q (A) and R269Q (B) (P2 currents at +50 mV). Peak data points fit with a single exponential relationship with time constant indicated. (C) Comparison of mean τ_{rec} values at HP=−100 mV. WT, R293A, and R296A data acquired previously [21]. R293Q (n=6), R296Q (n=8).

(Fig. 11B) resulted in the following values: R290A: $q_{rec,csi}=0.99e_0$; R290Q $q_{rec,csi}=0.60e_0$.

4. Discussion

Previous analysis of putative gating charge elimination in Kv4.3 S4 was, to the best of our knowledge, the first experimental demonstration in any Kv4 channel that positive charges in this domain are associated with voltage-dependent gating transitions. Our present results confirm and expand upon these results, and argue that S4 positively charged residues play a more complicated role in the regulation of gating in Kv4.3 than in Kv1 channels. Closed-state inactivation (CSI) appears to result from inherent voltage-sensitive gating transitions or novel coupling mechanisms to S4-mediated activation gating. Such processes occur prior to the final closed-to-open state transition, and cannot be accounted for by the conventional Shaker model of channel gating [10,11,23,24]. We propose that these processes, which would predominate at less depolarized potentials, result in uncoupling or block of VSD interaction with the S6 activation gate, or block the preactivated pore domain (S5–S6).

We acknowledge that use of a two state model is simplistic and that calculated effective gating charge values displayed in Tables 1–4 are minimal estimates (see Methods). Our assignment of "predominant effect(s)" of a specific mutant as summarized in Tables 1 and 3 is subject to the same limitations. We also acknowledge that analysis of

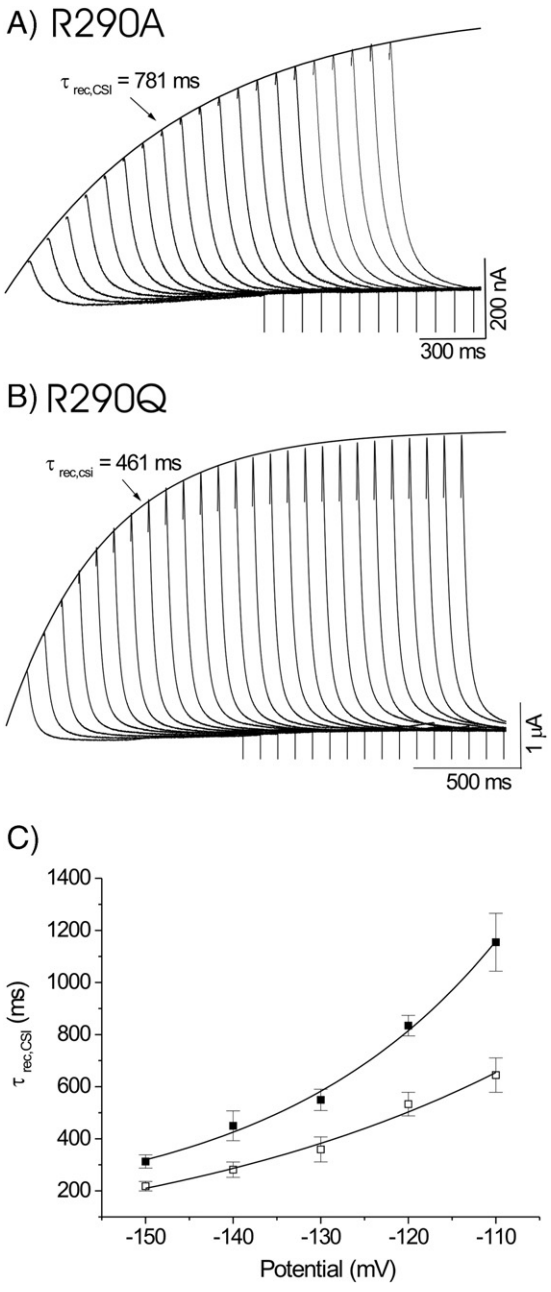

Fig. 11. Recovery from CSI developed at HP=−100 mV for R290A and R290Q. See text for protocol details. (A) Representative R290A recovery from CSI waveform measured at −120 mV. Peak P2 currents (elicited at +50 mV) fit as a single exponential function with time constant indicated. (B) Representative R290Q recovery from CSI waveform measured at −120 mV. Peak P2 currents (elicited at +50 mV) fit as a single exponential function with time constant indicated. (C) Mean $\tau_{rec,csi}$ $-V_m$ relationships for R290A (solid, n=5) and R296Q (hollow, n=6). Curve fits: R290A: $117.1\,e^{\frac{mV}{25.52}}+98.0$ ms; R290Q: $118.7e^{\frac{mV}{43.91}}+89.1$ ms.

additional mutants may provide important insights. Determining the effects of corresponding R → K (lysine) and R → M (methionine) mutants may be informative, as R → K reduces side chain volume by18.8 cm^3/mol while maintaining net positive charge. R → M removes this charge and similarly reduces side chain volume by 22 cm^3/mol. Mutagenesis of uncharged residues may also provide important mechanistic clues. Future studies may address these issues. Nonetheless, while our results should be viewed as qualitative, the overall trends they suggest for the roles that S4 arginine residues appear to play in the regulation of Kv4.3 gating transitions, and CSI and recovery in particular, are novel and important.

4.1. Activation and deactivation processes

Despite significant differences in residue properties, overall effects of corresponding R → A/Q mutant pairs on steady-state P_O were similar. Perturbation of structural properties was predominant at positions 290 and 296, but minimal at 293. Perturbation of electrostatic properties was also consistent at 290 and 293, and there was a general trend toward lesser reduction in q_{act} as residues were neutralized from the N-terminal to the C-terminal ends of S4. These findings suggest a model wherein R290 and R293 form electrostatic interactions important during the process of activation. However, there were differences in the predicted effects produced by the two mutant pairs at position 296. R296A predominantly resulted in structurally-mediated perturbations, whereas R296Q resulted in a combination of electrostatically- and structurally-mediated effects (Table 1). Previous work analyzing gating currents in Kv1 channels have indicated that single residue mutation in S4 can produce non-additive effects [17,18]. Similar effects may be responsible for the differences between R296A and R296Q noted here.

Due to the voltage clamp step rise time limitations of the two microelectrode voltage-clamp technique and our use of the 90% rise time criterion [20,21,38] (see Methods), measurements of activation and deactivation time constants are subject to technical limitations. Nonetheless, WT τ_{act}–V_m and τ_{deact} –V_m relationships (Fig. 4) are in good agreement with those reported previously by Wang et al. [19], who employed the more rapid cut open oocyte voltage clamp technique [43]. These investigators fit their τ_{act}–V_m curve as a double exponential function and reported minimal effective q_{act} values of $0.27e_0$ and $2.11e_0$, suggesting the existence of two populations of Kv4.3 activation gating charge. Our kinetic estimate of $q_{act} = 1.56e_0$, derived from fitting the τ_{act}–V_m curve to a single exponential function, is between the high-intermediate range of the two values reported previously [19]. The issue of bi-exponential voltage dependence of WT activation kinetics will need to be addressed in future studies.

Similar to steady-state analyses, kinetic measurements argue for the importance of electrostatic and structural characteristics of native residues in Kv4.3 activation. However, the two analytical approaches did not yield consistently similar results. For example, while all R → A/Q mutant pairs reduced q_{act}, kinetic analysis indicated that neutralization of C-terminal-most R296 produced the largest reduction in q_{act} (Table 2), in contrast to steady-state predictions (Table 1). While these differences may be due to limitations of our measurements, they may also be due to inherent limitations of our analysis. Thermodynamic predictions of the two-state model assume that gating transitions occur instantaneously. However, a non-instantaneous reaction pathway exists, indicating the presence of at least one high-intermediate energy transition state that determines gating transition rates. Our results provide evidence that variation in residue properties may selectively alter interactions within unique microenvironments, either lipid, aqueous, and/or proteinaceous, encountered during S4-mediated forward versus reverse gating transitions [14–16]. This raises the possibility that future pharmacologic or mutagenic maneuvers may be developed to selectively alter CSI or recovery characteristics with minimal effects on activation.

4.2. Inactivation and recovery characteristics

WT q_{csi} values were 2.3-times larger than q_{act} values. However, while mean q_{act} values (Table 1) were obtained from single subunit "*a*" relationships, it is unclear if corresponding "*i*" relationships reflect the behavior of single or multiple subunits. This uncertainty may account for the higher q_{csi} values noted. Nonetheless, two general trends emerged: i) all mutants reduced q_{csi}, suggesting prominent perturbation of electrostatic properties; and ii) with the exception of R296Q, all mutants significantly stabilized inactivated closed states, suggesting structural characteristics were altered.

Papazian et al. [26] first demonstrated that Shaker S4 mutants produced similar and parallel shifts in both activation and inactivation relationships, consistent with the idea that the two processes are coupled. This proposal has been subsequently verified and demonstrates that the apparent voltage dependence of inactivation arises out of the kinetics of activation [24]. In contrast, our results are consistent with the proposal that arginine residues in S4 either impart inherent voltage sensitivity to closed-state inactivation [3,9,20,21,44], or that CSI is coupled to activation by a mechanism unique from Shaker. While the hyperpolarizing shifts in both "a^4" and "*i*" produced by R290A/Q are consistent with partial coupling, effects of the mutant pairs at positions 293 and 296 did not consistently parallel one another. R296Q, in particular, revealed similar trends to R296A with respect to steady-state activation, but unique effects with respect to "*i*". We therefore propose that R293 and R296 are residues critically involved in regulating CSI.

While each R → A mutant slowed deactivation, R293Q and R296Q partially restored WT kinetics. Combined with data presented here and previously [21], we have additional evidence on the effects of KChIP2 coexpression [3,9] and changes in extracellular potassium concentration [9] which suggests that recovery may be coupled to deactivation. All of these maneuvers produced similar and paralleling effects on both deactivation and recovery kinetics. Although R293Q modestly accelerated deactivation kinetics as compared to WT (Fig. 6B) but still slowed recovery (Fig. 10), the kinetics of macroscopic recovery were significantly faster for both R293Q and R296Q than their corresponding A constructs (Fig. 10). This argues for important structural roles of these residues in regulating both CSI and deactivation-recovery coupling. Therefore, while we presently cannot explain the anomalous effects of R293Q, our results overall support the proposal that recovery from inactivation is coupled to deactivation. These results also raise an important question: if mutation at positions 293 and 296 do, in fact, uncouple CSI from activation, how can R293Q and R296Q partially restore WT recovery kinetics? We hypothesize that the underlying mechanisms may reside in the interactions of the incorporated residue within unique microenvironments experienced during forward and reverse gating transitions. Further, non-native residues may adjust the focal point of the transmembrane electrical field (discussed below).

4.3. Implications for potential interactions and comparative Kv channel structure–function relationships

There are presently two contending models for voltage-sensitive S4 transitions in Kv1 channels, the "helical screw" and "transporter" models [14–16,45]. Although details differ between the two, both models propose the existence of two aqueous membrane crevices, one accessible from the extracellular surface and the other from the intracellular surface. These two crevices would focus the transmembrane electrical field to a narrow hydrophobic septum [13–16,30–32]. Such focusing would permit relatively small movements of S4 to generate comparatively large gating currents. Furthermore, gating transitions would continually refocus the transmembrane electric field along narrow regions of S4, initially across R1 in the closed state, and subsequently across R4 in the open state [13–16]. Within the

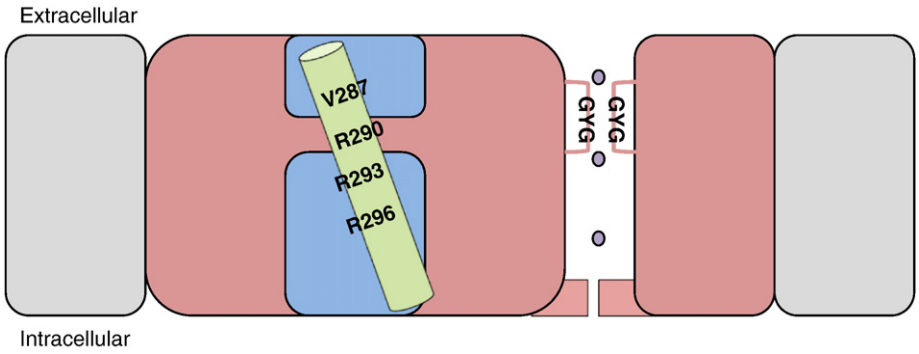

Fig. 12. Cartoon illustration of the position of S4 (green) relative to membrane crevices (blue) in the closed-state of Kv4.3. In contrast to Kv1 channels, we propose that the transmembrane electrical field is focused across R290 (R2 in Kv1). This would suggest that the outer membrane crevice is either deeper or thicker than in Kv1, allowing the field to influence arginine at this position. Lipid bilayer shown in gray, channel complex in red, and potassium ions in the pore shown in purple.

framework of such a model, recent studies on Kv1 channels have suggested that during activation S4 is displaced by 6–8 Å while simultaneously rotating ~180° [34–36]. As a result, the dielectric and chemical properties of the immediate microenvironment experienced by individual gating charges may vary significantly during channel transitions [14–16,30–36] Our results suggest that side chain interactions are particularly prominent during the reverse gating transitions of deactivation and recovery.

The absence of R1 in Kv4.3 may have important mechanistic consequences for understanding differences in gating characteristics between Kv1 and Kv4 channels [1–3]. We have previously mapped the Kv4.3 sequence upon the crystal structure of the open state conformation of Kv1.2 [21,46,47]. This suggested that in the open state R290 would face either the outer membrane interface or an aqueous crevice partially formed by S5 of the adjacent subunit, while R293 and R296 would face an aqueous crevice formed by S1, S2, and/or S3. None of the putative gating charge residues would be directly exposed to energetically unfavorable hydrophobic surroundings in the open state [48,49]. However, the presence of V287 would eliminate an energetic constraint at this position, and likely favor localized hydrophobic interactions. The presence of F286 immediately upstream of V287 (Fig. 1A) further supports this proposal. These considerations could allow the register of S4 in the open state to be different in Kv4.3 versus Kv1.2, as well as alter the properties of the external crevice and hydrophobic septum.

The crystal structure of the closed state of a Shaker-like channel has yet to be solved, but three closed state models have been proposed [34,36,50]. That of Campos et al. [34] in support of a minimal model of the Shaker closed state is particularly compelling. This model (which used the structure of the Kv1.2 open state as a constraint) proposes that R1 and R2 are positioned in the outer half of the membrane, oriented towards S1–S3, and lie in close proximity to hydrophobic isoleucine residues in S1 and S2. This microenvironment would correspond to the hydrophobic septum separating the two crevices of the gating pore, and would serve to focus the electric field across R1. The importance of L361, which immediately precedes R1 in Shaker, in positioning S4 in the resting channel has also been demonstrated [51]. R3 and R4 would each be positioned in the intracellular half of the membrane and exposed to the intracellular crevice. The role of S3 is not accounted for in this model.

Applying this model to Kv4.3, F286 may form part of the hydrophobic septum, implying that at resting potentials the electric field would be focused over a region of S4 lacking positive charge. Long et al. [50] used chimaeric Kv2.1–Kv1.2 channels to propose that phenylalanine F233 in S2, which is positioned three residues "below" corresponding Shaker I287, forms the septum. Kv4.3 has a comparable phenylalanine: F237 in S2. To accommodate these considerations, we propose that the outer crevice in Kv4.3 is either deeper than in Kv1 channels, which would focus the field across R290 in the closed state, or is thicker, which would diffuse the electrical field but still allow it to influence R290, thus reducing voltage sensitivity at this position (Fig. 12).

4.4. Concluding remarks

We propose that transitions in the Kv4.3 VSD, in particular those mediated by S4 arginine residues at positions 290, 293, and 296, may be responsible for regulating not only activation and deactivation processes, but also those of closed-state inactivation and recovery from inactivation. Our results suggest that CSI either possesses inherent voltage dependence, or that apparent voltage dependence arises from coupling to activation by a mechanism significantly different from that noted in Kv1 channels. These proposals are consistent with recently reported correlations between CSI and gating charge immobilization in modified CTX-sensitive Kv4.2 channels [41] (see Methods). However, our results further indicate that depending upon the specific residue analyzed, perturbation of electrostatic, structural, or both properties can significantly alter specific Kv4.3 gating transitions. While underlying mechanisms of Kv4 channel CSI and recovery remain unresolved, data suggesting that S4 may regulate these processes is compelling.

Acknowledgements

We wish to acknowledge support provided by the American Heart Association (Founder's Affiliate Predoctoral Fellowship to MRS) and the UB School of Medicine and Biomedical Sciences, Department of Physiology and Biophysics (DLC). We also wish to thank Ms. Rachael Brust (Harvard Medical School, Biological and Biomedical Sciences) and Ms. Johanna Schwingel (UB School of Medicine and Biomedical Sciences, Department of Microbiology and Immunology) for technical assistance relating to this work.

References

[1] S.G. Birnbaum, A.W. Varga, L-Y. Yuan, A.E. Andersen, J.D. Sweatt, L.A. Schrader, Structure and function of Kv4-family transient potassium channels, Physiol. Rev. 84 (2004) 803–833.
[2] H.H. Jerng, P.J. Pfaffinger, M. Covarrubias, Molecular physiology and modulation of somatodendritic A-type potassium channels, Mol. Cell. Neurosci. 27 (2004) 343–369.
[3] S.P. Patel, D.L. Campbell, Transient outward potassium current, "I_{to}", phenotypes in the mammalian left ventricle: underlying molecular, cellular and biophysical mechanisms, J. Physiol. 569 (2005) 7–39.
[4] S.M. Thompson, I_A in play, Neuron 54 (2007) 850–852.
[5] J. Kim, S.-C. Jung, A.M. Clemens, R.S. Petralia, D.A. Hoffman, Regulation of dendritic excitability of activity-dependent trafficking of the A-type K^+channel subunit Kv4.2 in hippocampal neurons, Neuron 54 (2007) 933–947.
[6] H.-J. Hu, Y. Carrasquillo, F. Karim, W.E. Jung, J.M. Nerbonne, T.L. Schwarz, R.W. Gereau, The Kv4.2 potassium channel subunit is required for pain plasticity, Neuron 50 (2006) 89–100.

[7] R. Sah, R.J. Ramirez, G.Y. Oudit, D. Gidrewicz, M.G. Triveri, C. Zoble, P.H. Backx, Regulation of cardiac excitation–contraction coupling by action potential repolarization: role of the transient outward potassium current (I_{to}), J. Physiol. 546 (2003) 5–18.
[8] R. Bahring, L.M. Boland, A. Vargese, M. Gebauer, O. Pongs, Kinetic analysis of open- and closed-state inactivation transitions in human Kv4.2 A-type potassium channels, J. Physiol. 535 (2001) 65–81.
[9] C.C. Amadi, R.D. Brust, M.R. Skerritt, D.L. Campbell, Regulation of Kv4.3 closed state inactivation and recovery by extracellular potassium and intracellular KChIP2b, Channels 1 (2007) 305–314.
[10] R.W. Aldrich, Fifty years of inactivation, Nature 411 (2001) 643–644.
[11] M. Zhou, J.H. Morals-Cabral, S. Mann, R. MacKinnon, Potassium channel receptor site for the inactivation gate and quaternary amine inhibitors, Nature 411 (2001) 657–661.
[12] F. Bezanilla, The voltage-sensor in voltage-dependent ion channels, Physiol. Rev. 80 (2000) 555–592.
[13] F. Bezanilla, Voltage-gated ion channels, IEEE Trans. Nanobiosci. 1 (2005) 34–48.
[14] F. Bezanilla, How membrane proteins sense voltage, Nature Rev. Mol. Cell. Biol. 9 (2008) 323–332.
[15] F. Tombola, M.M. Pathak, E.Y. Isacoff, How does voltage open an ion channel? Ann. Rev. Cell. Dev. Biol. 22 (2006) 23–52.
[16] B. Chanda, F. Bezanilla, A common pathway for charge transport through voltage-sensing domains, Neuron 57 (2008) 345–351.
[17] S.K. Aggarwal, R. MacKinnon, Contribution of the S4 segment to gating charge in the Shaker K^+channel, Neuron 16 (1996) 1169–1177.
[18] S.A. Seoh, D. Sigg, D. Papazian, F. Bezanilla, Voltage-sensing residues in the S2 and S4 segments of the Shaker K_+channel, Neuron 16 (1996) 1159–1167.
[19] S. Wang, V. Bondarenko, Y. Qu, M.J. Morales, R.L. Rasmusson, H.C. Strauss, Activation properties of Kv4.3 channels: time, voltage and $[K^+]_o$ dependence, J. Physiol. 557 (2004) 705–712.
[20] S.P. Patel, R. Parai, R. Parai, D.L. Campbell, Regulation of Kv4.3 voltage-dependent gating kinetics by KChIP2 isoforms, J. Physiol. 557 (2004) 19–41.
[21] M.R. Skerritt, D.L. Campbell, Role of S4 positively charged residues in the regulation of Kv4.3 inactivation and recovery, Am. J. Physiol. Cell. Physiol. 293 (2007) C906–C914.
[22] F.J. Sigworth, Voltage gating of ion channels, Quart. Rev. Biophys. 27 (1994) 1–40.
[23] G. Yellen, The moving parts of voltage-gated ion channels, Quart. Rev. Biophys. 31 (1998) 239–295.
[24] B. Hille, Gating: Voltage sensing and inactivation, Ion Channels of Excitable Membranes, 3rd Edition, Sinauer Associates, Sunderland, MA, 2001, pp. 603–634.
[25] M.B. Jackson, Global transitions in proteins, Molecular and Cellular Biophysics, Cambridge University Press, Cambridge, UK, 2006, pp. 1–24.
[26] D.M. Papazian, L.C. Timpe, Y.N. Jan, L.Y. Jan, Alteration of voltage dependence of Shaker potassium channel by mutations in the S4 sequence, Nature 349 (1991) 305–310.
[27] A.A. Zamyatnin, Amino acid, peptide, and protein volume in solution, Ann. Rev. Biophys. Bioeng. 13 (1984) 145–165.
[28] J. Kyte, R.F. Doolittle, A simple method for displaying the hydropathic character of a protein, J. Mol. Biol. 157 (1982) 105–132.
[29] D.M. Engelman, T.A. Steitz, A. Goldman, Identifying nonpolar transmembrane helices in amino acid sequences of membrane proteins, Ann. Rev. Biophys. Biophys. Chem. 15 (1986) 321–353.
[30] D.M. Starace, F. Bezanilla, A proton pore in a potassium channel voltage sensor reveals a focused electric field, Nature 427 (2004) 548–553.
[31] O.K. Asamoah, J.P. Wuskell, L.M. Loew, F. Bezanilla, A fluorometric approach to local electric field measurements in a voltage-gated ion channel, Neuron 37 (2003) 85–97.
[32] C.A. Ahern, R. Horn, Focused electric field across the voltage sensor of potassium channels, Neuron 48 (2005) 25–29.
[33] F. Tombola, M.M. Pathak, E.Y. Isacoff, Voltage-sensing arginines in a potassium channel permeate and occlude cation-selective pores, Neuron 45 (2005) 379–388.
[34] F.V. Campos, B. Chanda, B. Roux, F. Bezanilla, Two atomic constraints unambiguously position the S4 segment relative to S1 and S2 segments in the closed state of Shaker K channel, Proc. Nat. Acad. Sci. 104 (2007) 7904–7909.
[35] F. Tombola, M.M. Pathak, P. Gorostiza, E.Y. Isacoff, The twisted ion-permeation pathway of a resting voltage-sensing domain, Nature 445 (2007) 546–549.
[36] M.M. Pathak, V. Yarov-Yarovoy, G. Agarwal, B. Roux, P. Barth, S. Kohout, F. Tombola, E.Y. Isacoff, Closing in on the resting state of the Shaker K^+ channel, Neuron 56 (2007) 124–140.
[37] S.P. Patel, D.L. Campbell, M.J. Morales, H.C. Strauss, Heterogeneous expression of KChIP2 isoforms in the ferret heart, J. Physiol. 539 (2002) 649–656.
[38] D.L. Campbell, R.L. Rasmusson, Y. Qu, H.C. Strauss, The calcium-independent potassium current in isolated ferret right ventricular myocytes. I. Basic characterization and kinetic analysis, J. Gen. Physiol. 101 (1993) 571–601.
[39] L.A. Kim, J. Furst, M.H. Butler, S. Xu, N. Grigorieff, S.A. Godstein, I^+_{to}channel-interacting protein 2, J. Biol. Chem. 279 (2004) 5549–5554.
[40] K. Dougherty, M. Covarrubias, A dipeptidyl aminopeptidase-like protein remodels gating charge dynamics in Kv4.2 channels, J. Gen. Physiol. 128 (2006) 745–753.
[41] K. Dougherty, J.A. De Santiago-Castillo, M. Covarrubias, Gating charge imobilization in Kv4.2 channels: The basis of closed-state inactivation, J. Gen. Physiol. 131 (2008) 257–273.
[42] A.L. Hodgkin, A.F. Huxley, A quantitative description of membrane current and its application to conduction and excitation in nerve, J. Physiol. 117 (1952) 500–544.
[43] E. Stefani, F. Bezanilla, Cut-open oocyte voltage-clamp technique, Methods Enzymol. 293 (1998) 300–318.
[44] S. Wang, V.E. Bondarenko, Y.-J. Qu, G.C. Bett, M.J. Morales, R.L. Rasmusson, H.C. Strauss, Time-and voltage-dependent components of Kv4.3 inactivation, Biophys. J. 89 (2005) 3026–3041.
[45] W.A. Catterall, Molecular properties of voltage-sensitive sodium channels, Ann. Rev. Biochem. 55 (1986) 953–985.
[46] S.B. Long, E.B. Campbell, R. MacKinnon, Crystal structure of a mammalian voltage-dependent Shaker family K^+ channel, Science 309 (2005) 897–903.
[47] S.B. Long, E.B. Campbell, R. MacKinnon, Voltage sensor of Kv1.2: structural basis of electromechanical coupling, Science 309 (2005) 903–908.
[48] A. Parsegian, Energy of an ion crossing a low dielectric membrane: Solutions to four relevant electrostatic problems, Nature 221 (1969) 844–846.
[49] L. Li, I. Vorobyov, A.D. MacKerell, T.W. Allen, Is arginine charged in a membrane? Biophys. J. 94 (2008) L11–L13.
[50] S.B. Long, T. Xiao, E.B. Campbell, R. MacKinnon, Atomic structure of a voltage-dependent K^+ channel in a lipid membrane-like environment, Nature 450 (2007) 376–383.
[51] Y.-C. Yang, C.-J. Own, C.-C. Kuo, A hydrophobic element secures S4 voltage sensor in position in resting Shaker K^+ channels, J. Physiol. 582 (2007) 1059–1072.